From simple to complex networks: Inherent structures, barriers, and valleys in the context of spin glasses

Z. Burda

M. Smoluchowski Institute of Physics, Jagellonian University, Reymonta 4, PL-30-059 Krakow, Poland

A. Krzywicki

Laboratoire de Physique Théorique, bâtiment 210, Université Paris-Sud, F-91405 Orsay, France

O. C. Martin

Laboratoire de Physique Théorique et Modèles Statistiques, bâtiment 100, Université Paris-Sud, F-91405 Orsay, France

Z. Tabor

Department of Biophysics, Collegium Medicum, Jagellonian University, PL-31-531 Krakow, Poland

Given discrete degrees of freedom (spins) on a graph interacting via an energy function, what can be said about the energy local minima and associated inherent structures? Using the lid algorithm in the context of a spin glass energy function, we investigate the properties of the energy landscape for a variety of graph topologies. First, we find that the multiplicity N_s of the inherent structures generically has a log-normal distribution. In addition, the large volume limit of $\ln\langle N_s\rangle/\langle \ln N_s\rangle$ differs from unity, except for the Sherrington-Kirkpatrick model. Second, we find simple scaling laws for the growth of the height of the energy barrier between the two degenerate ground states and the size of the associated valleys. For finite connectivity models, changing the topology of the underlying graph does not modify qualitatively the energy landscape, but at the quantitative level the models can differ substantially.

PACS number(s): 89.75.Fb, 75.10.Nr, 75.40.Mg

I. INTRODUCTION

Graphs and networks are a subject of study on their own, and more recently the possibility of doing statistical mechanics on these kinds of structures has been investigated. In many of the corresponding models, even though the local minima of the energy function proliferate, one knows little about their numbers or about their organization. Such properties are usually studied within the "energy landscape" paradigm which embodies both energetic and entropic effects. In fact, a complete knowledge of this landscape tells one everything about low energy excitations; that kind of information can be precious for understanding both equilibrium and out of equilibrium low temperature properties. This is especially true for "complex" systems that exhibit glassy behavior; these arise in many subjects of research, ranging from material science to protein folding.

Our purpose here is to find out how the "shape" and the scaling properties of such energy landscapes depend on the structure of the underlying graph when the Hamiltonian function is of the spin glass type. For this purpose, we shall consider four types of random graphs (cf. Refs. [1–4]). Previous studies have considered the thermodynamics of these systems: at high temperature the system is paramagnetic, and at low temperature there is a spin glass phase in which the magnetizations of the spins freeze in apparently random directions. However, relatively little attention has been put into energy landscape questions when the underlying graphs are random. In particular, nearly all previous landscape work on our classes of graphs has been limited to the Sherrington-

Kirkpatrick (SK) case [4]: the inherent structures (referred to as metastable states in the spin glass community) have been tackled analytically [5], and barrier sizes have been considered indirectly, either via free-energy barriers near the critical temperature [6], or by numerical studies of relaxation kinetics in Monte Carlo simulations [7,8]. Finally, there is very little work on the size of the ground-state valleys associated with the configurations that are reachable when staying below a given barrier. For all of our random graph ensembles, we shall first consider all configurations, enumerating the inherent structures as a function of their energy. We shall also use the lid algorithm [9–11] to obtain all configurations connected to the ground state while staying below a given energy; this gives the barrier to go from the ground state to its inverted pair and the size of the associated basin. In spite of the modest graph sizes considered, a considerable amount of information on these observables (and in particular their scaling laws) can be reliably extracted.

The paper is organized as follows. The models are defined in Sec. II. Then we examine all the local minima of the Hamiltonian and study their statistics (Sec. III). In Sec. IV we investigate in detail the scaling of the energy barrier separating the two degenerate ground states of these systems. We also extract the size of the valley around each ground state. We conclude in Sec. V.

II. MODELS

A. Geometry: Random graphs

A first component of our models consists of a graph on whose N vertices the spins will reside. We consider four

classes of graphs with markedly different topologies.

(1) Random *k*-regular (KR) graphs, where the degree (connectivity) of each node is fixed to *k*.

(2) Erdös-Rényi (ER) graphs, where each edge is put down with probability $p = \alpha/N$; as a result, at large *N*, the degree of a vertex is a Poisson distributed variable of mean α.

(3) Barabasi-Albert (BA) scale-free graphs generated by the usual growth process with the preferential attachment property [12]. Here, at large *N*, the degree distribution has a fat tail. In contrast to the previous graphs, the graphs in this class are highly inhomogeneous.

(4) Complete (i.e., fully connected) graphs. Here, the number of edges is no longer linear in *N*, but quadratic.

B. Matter: Frustrated Ising spins

To each edge *ij* of the underlying graph, we independently assign a weight J_{ij} according to a distribution symmetrized about 0, so both signs arise with equal probability. These elements, i.e., the random edges and their associated weights J_{ij}, define the system's "quenched disorder." The statistical mechanics problem arises when one assigns degrees of freedom to each site and has them interact. Here we put an Ising spin σ_i on each site *i*; the system's Hamiltonian is taken to be

$$H(\{\sigma_i\}) \equiv -\sum_{\langle ij \rangle} J_{ij}\sigma_i\sigma_j, \qquad (1)$$

where the sum runs over all pairs of sites connected by an edge of the graph. If not stated otherwise the weights J_{ij} are generated from a Gaussian distribution. This Hamiltonian defines a spin glass, the frustration coming from the fact that in general not all terms in the energy function can be simultaneously at their minimum. There is an obvious global $Z(2)$ symmetry corresponding to flipping simultaneously all the spins. Finally, because the J_{ij} are identical independently distributed and continuous random variables, generically there are just two degenerate ground states (related by a global spin flip).

We shall be interested in the large *N* limit, in which case it is appropriate to keep the system's energy extensive. For instance in the SK model [4] one sets $\mathrm{var}(J_{ij}) = O(1/N)$. More generally, if the mean connectivity grows, we want to keep the energy density from diverging; in all that follows we shall thus take

$$\mathrm{var}(J_{ij}) = \frac{J^2}{\langle k \rangle}, \qquad (2)$$

where $\langle k \rangle$ is the average graph degree. This choice of scale eliminates trivial differences between the values of the same observables in distinct models, allowing for a more direct comparison.

C. Algorithmic procedures

The 2^N configurations of the spin glass are conveniently represented by vertices of an *N*-dimensional Boolean hypercube: each vertex is identified by a binary number
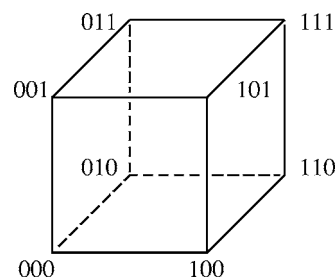

FIG. 1. Boolean (hyper)cube representing the possible configurations of a three-spin system ($N=3$).

$0, \ldots, 2^N - 1$ of *N* bits, a bit value of 1 (0) at the *i*th position corresponding to the *i*th spin being up (down). Neighbor vertices differ in exactly one bit (see Fig. 1, where the case $N = 3$ is illustrated). To each configuration (vertex of the hypercube) we associate the energy calculated from the Hamiltonian (1). The set of vertices of the Boolean hypercube is our configuration space; these and their associated energies define an energy landscape, the object of our study. If a vertex has an energy strictly lower than that of all of its nearest neighbors, the configuration is "one-spin-flip stable" and hereafter will be referred to as an *inherent structure*. (As mentioned previously, such configurations are sometimes called "metastable states.") We use this vocabulary, proper to landscape studies, in the spin glass context. Note that no gradient algorithm (like those refered to when inherent structures were originally defined on systems with continuous variables) will be employed in this work.

One instance of a problem is created by generating a random graph in the desired class with *N* vertices followed by the generation of the set of weights J_{ij}. The energy landscape of that instance is then probed using algorithms which examine all configurations, their energies, etc. The process is then repeated for as many instances as possible so statistical properties can be inferred. Finally, one studies the *N* dependence to extract the large *N* scaling laws.

For $N \le 32$, a single PC machine word suffices to store the whole bit sequence representing a configuration on the Boolean hypercube, and furthermore many of the operations on configurations are easily implemented as binary operators on the corresponding machine words. In practice, $N \approx 30$ turns out to be a natural performance limit for our programs since for larger *N* the enumeration of all 2^N configurations takes too much computation time.

The exhaustive enumeration of all inherent structures is in principle straightforward. On a 2 GHz PC, it requires a few hundred seconds of CPU time for a single instance of 30 spins. The determination of the height of the energy barrier separating the two degenerate ground states is more time consuming. We use for this purpose a variant of the lid algorithm [13]. Starting from just one of the two degenerate ground states, one iteratively steps to neighboring configurations as long as their energy is below a prescribed "lid" value. Using a pictorial analogy, one can imagine water spreading out in a mountainous landscape: Given the source at the chosen ground state, the water will "wet" neighboring sites of the hypercube iteratively as long as their energy is below that of the lid. Following this process, the water front

TABLE I. Slope of the least-square linear fit of $\ln\langle N_s\rangle$ ($\langle\ln N_s\rangle$) versus N. Only statistical errors are estimated; the lower figure for k $=2$ is the exact value. The fact that for the SK model the lower figure is slightly larger than the upper one is a finite size artifact reflecting the decrease with N of the variance of $\ln N_s$ discussed in the text.

	KR ($k=2$)	KR ($k=4$)	ER $\langle k\rangle=4$	BA ($m=2$)	BA ($m=1$)	SK
Slope of $\ln\langle N_s\rangle$	0.2417(3)	0.2179(2)	0.2029(2)	0.1787(3)	0.1640(4)	0.1988(2)
Slope of $\langle\ln N_s\rangle$	0.2310490	0.2163(2)	0.1997(2)	0.1728(3)	0.1510(3)	0.2008(2)

progresses continuously, submerging successive sites until a pool is formed. There exists a critical value of the lid beyond which the water can pour into the basin belonging to the mirror ground state. This is the barrier we shall be investigating. The computer program calculates not only the height of the barrier, but also the area of the pool (the number of wet sites) just before the leaking begins, and the Hamming distance from the source to the pass or passes leading to the mirror basin. We refer to this basin as the ground-state valley.

The time needed to execute this code for one instance of 30 spins takes from a few hundred to several thousand seconds and strongly depends on the geometry of the model. For example, for BA graphs it is about 3300 s. This time is even longer for regular graphs with $k=2$: the ground-state valley is often very large and the algorithm needs much time to fill it and to reach the pass leading to the other ground state.

III. INHERENT STRUCTURES

A. The case of ring geometry

We first consider the case of ring geometry as it will allow us to understand the generic behavior of most of the other models. We thus consider a graph that is a ring with N spins and periodic boundary conditions: this corresponds in fact to a particular ($k=2$)-regular graph and it is easy to see that the properties we shall obtain are also those of this class of graphs (where one generally has several rings).

A configuration $\{\sigma_i\}_{i=1,\ldots,N}$ is an inherent structure if and only if each of its spins is parallel to its local field. To describe such a configuration, it is convenient to focus on

$$x(i, i+1) = \sigma_i J_{i,i+1}\sigma_{i+1}. \tag{3}$$

When $x(i, i+1) > 0$, the bond $(i, i+1)$ is satisfied, otherwise it is unsatisfied. An unsatisfied bond corresponds to having a domain wall (after resorting to a gauge transformation). Note that because of the periodic boundary conditions imposed, the number of domain walls in all configurations has the same parity as in the ground state.

In an inherent structure, if $x(i, i+1) < 0$, then necessarily $x(i-1, i) > |x(i, i+1)| < x(i+1, i+2)$. These conditions are equivalent to having (i) $|J_{i-1,i}| > |J_{i,i+1}| < |J_{i+1,i+2}|$, plus (ii) the two neighboring bonds of the unsatisfied bond $(i, i+1)$ must be satisfied. Let M be the number of bonds $(i, i+1)$ for which these last two properties hold. Then, there are M possible binary choices (either passing or not passing a domain wall through each of the bonds), leading to a number of inherent states $N_s = 2^M$, a result derived over two decades ago [14,15].

For any given instance of the J_{ij}, one can easily determine the set of bonds $(i, i+1)$ satisfying $|J_{i-1,i}| > |J_{i,i+1}| < |J_{i+1,i+2}|$. Although no two such bonds can be adjacent, the correlations are short range. As a consequence, the number M of these bonds is extensive as well as their variance. In fact, M is asymptotically distributed as a Gaussian random variable according to the central limit theorem. Furthermore, it can be shown [14,15] that for any continuous distribution of the J_{ij}, one has the remarkable property

$$\lim_{N\to\infty}\frac{\langle M\rangle}{N} = \frac{1}{3}. \tag{4}$$

Since $N_s = 2^M$, we obtain

$$\lim_{N\to\infty}\frac{\langle\ln N_s\rangle}{N} = \frac{\ln 2}{3} = 0.231049\ldots \tag{5}$$

as indicated in Table I. Finally, given that M is Gaussian, N_s follows a log-normal distribution at large N.

This simple example allows us to guess what happens in other finite connectivity models. The role of the localized domain wall should be replaced by a local cluster of spins that can flip [16]. If there are M such clusters, the number of inherent states will be roughly 2^M; finally, if as expected M is a Gaussian random variable at large N, then N_s will be log normal.

B. The mean multiplicity

For all our models we find that the number N_s of inherent structures grows exponentially with N. Earlier analytic work [5,17–19] has established this for regular graphs (including the complete ones). We recover these results numerically, extending them to scale-free graphs (see Fig. 2).

The slope of $\ln\langle N_s\rangle$ versus N is given in Table I for a sample of models. We recall that the analytic result [5,17,18]
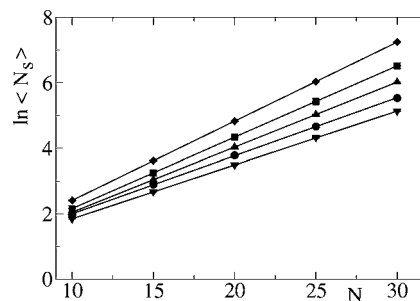

FIG. 2. Plot of $\ln\langle N_s\rangle$ versus N and associated linear fits. Diamonds, KR ($k=2$); squares, KR ($k=4$); up triangles, SK; circles, BA ($m=2$); down triangles, BA ($m=1$).
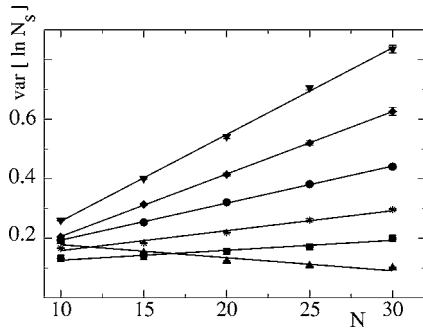
FIG. 3. The plot of $\text{var}(\ln N_s)$ versus N (linear regression). Down triangles, BA ($m=1$; tree); diamonds, KR ($k=2$); circles, BA ($m=2$); stars, ER ($\langle k \rangle=4$); squares, KR ($k=4$); up triangles, SK.

FIG. 4. The multiplicity distribution for the regular $k=4$ geometry (histogram with bin size$=100$). The ordinate is the value of N_s for an instance. (Summed over our instances with $N=30$, we have a total of 10 105 instances; note the events at large N_s arising from just one instance.) The solid curve is the log-normal function with the same mean and variance as in the numerical data.

for the SK model is 0.1992…, to be compared with 0.1988(2) read from our table. We find this agreement remarkable and encouraging, indicating that reliable results can be obtained from rather small systems. We also reproduce a qualitative result of Ref. [19]: for regular graphs the slope *decreases* with increasing connectivity. (Note that we cannot compare our figures quantitatively with the analytic predictions of Ref. [19] because the definitions of metastable states used are different.) In contrast, this trend with connectivity is *not* found in inhomogeneous graphs of the BA type, where the slope is *larger* for $m=2$ than for $m=1$ (m is the number of links attached in one step of the growth process; thus the average connectivity equals $2m$ up to finite size corrections). Note that the case $m=1$ produces tree networks (that is, no loops are generated).

It is also of interest to consider the average of $\ln N_s$ rather than the logarithm of the average. The results for these averages also show a clean linear behavior with N, and the slopes are given in Table I. We see that in all cases, the two values are numerically close; the potential differences will be discussed in Sec. III D.

C. The multiplicity distribution

The exponential growth of N_s with N indicates that $\ln N_s$ is an extensive quantity. For finite connectivity models it is natural to guess that this "entropy" arises from localized excitations [16] that are extensive in number. Indeed, starting with a ground state, one expects to have an extensive number of small sized clusters (say of just two spins as an example) that can be flipped while keeping each spin parallel to its local field. (The corresponding modified configuration then remains an inherent structure.) Furthermore, this "gas of clusters" should be weakly interacting. (We thus have a generalization of what happened in the ring geometry, although it was domain walls that played the role of the localized objects there.) This picture should hold for all finite connectivity models so we focus on those first, postponing the discussion of the SK model to later.

If one can excite an extensive number of clusters and if these interact only weakly, we expect not only the mean but also the variance of $\ln N_s$ to be linear in N. Our numerical data show that this is indeed the case as displayed in Fig. 3. The fits are good, especially when the slope is large. Now
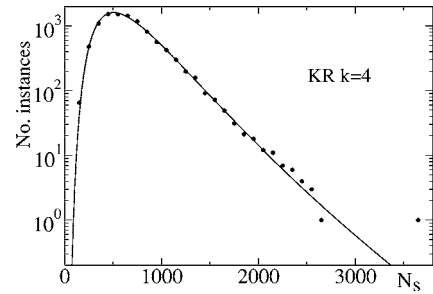
pushing the weakly interacting gas picture further, one expects a central limit theorem behavior for $\ln N_s$. We have thus calculated its higher order cumulants κ_3 and κ_4. Here the errors are rather large and so only the qualitative behavior with N can be extracted. The general trend is that the scaled cumulants, i.e., $\kappa_3/\sigma^{3/2}$ and κ_4/σ^2, are decreasing and probably go to zero at large N. (At $N=30$ they are both $\lesssim 0.1$.) All this indicates that the multiplicity distribution becomes *log normal* at large N:

$$P(N_s) \simeq \frac{\exp[-(\ln N_s - \langle \ln N_s \rangle)^2/2\sigma^2]}{N_s \sqrt{2\pi\sigma^2}} \qquad (6)$$

where σ^2 is the variance of $\ln N_s$. This distribution is illustrated for the KR $k=4$ model in Fig. 4. Similar results are obtained for other models (data not shown). The $k=2$ case is somewhat special since the multiplicities there are always equal to integer powers of 2 as we saw in the ring geometry.

D. The special case of the SK model

Now we move on to the SK model which behaves somewhat differently from the other models because of its infinite connectivity. Both $\ln\langle N_s \rangle$ and $\langle \ln N_s \rangle$ increase linearly with N, as already mentioned. The difference from the other models concerns the variance of $\ln N_s$; as shown in Fig. 3, this variance *decreases* as N grows. (The line displayed there is to emphasize the trend; the actual behavior is an inverse power law with N.) Note that the slope of the other models is always positive but decreases as their connectivity increases; for instance the slope is close to zero but definitely positive for the ER $\langle k \rangle=4$ model.

Neglecting the higher order cumulants of $\ln N_s$, one has

$$\ln\langle N_s \rangle = \langle \ln N_s \rangle + \frac{1}{2}\text{var}(\ln N_s). \qquad (7)$$

Thus, as $N \rightarrow \infty$, we have for our finite connectivity models

$$\frac{1}{N}[\ln\langle N_s \rangle - \langle \ln N_s \rangle] \rightarrow \text{const.} \qquad (8)$$

This shows that in such models, the two different kinds of averages are distinct, though their difference is numerically
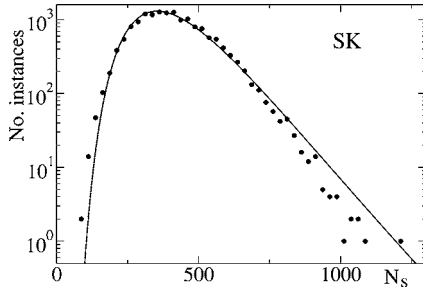
FIG. 5. The multiplicity distribution for the SK model. The ordinate is an instance's number of inherent structures (data for N =30 and 15 607 instances). The line is the log-normal curve with the same mean and variance of $\ln N_s$ as in the numerical data. Notice that in the tails the data deviate somewhat from the curve. As stated in the text, for SK the scaled higher order cumulants, although "small," are nevertheless about twice what they are in the other models.

rather small. However, for the SK model, the constant on the right hand side is zero because the variance is subextensive. This justifies why we find $\langle \ln N_s \rangle$ to be so close to $\ln \langle N_s \rangle$, in agreement with the theoretical result that the two averages coincide in the thermodynamic limit. This particular property seems to be specific to the SK model because of its infinite connectivity.

How can these results be understood? Clearly we cannot rely on the simple picture derived from localized clusters because in the SK model every spin is interacting with every other one. Do low energy excitations nevertheless consist of just a few spins? To find out, recall [20] that in the ground state, the field h_i experienced by a spin σ_i has a distribution $P(h_i) \approx |h_i|$ at small fields; thus small fields are *rare*. Because of this, the number of two-spin excitations that will produce an inherent structure is only $O(1)$! Going from 2 to k spins increases this number; in fact it becomes exponentially large in k. Because of this, one is driven to $k=O(N)$ so the vast majority of inherent structures correspond to excitations with $O(N)$ flipped spins, explaining why $\ln N_s$ is extensive in the SK model. Furthermore, for such a large number of spin flips, the detail of the J_{ij} gets washed out. Thus one expects very little instance to instance fluctuation of $\ln N_s$, suggesting correctly that var($\ln N_s$) is small.

Finally, we have investigated the distribution of $\ln N_s$ (see Fig. 5). Surprisingly, just as in the finite connectivity models, it seems to be log normal, as indicated by the smallness of cumulants of order 3 and 4; these cumulants are rapidly decreasing with increasing N and are around 0.2 at $N=30$. We have no qualitative justification for this simple result.

E. The multiplicity as a function of energy

To get further insight, it is instructive to consider the dependence of the number of inherent structures as a function of their energy. We first define the scaled excitation energy per spin $\varepsilon = (E - E_0)/JN$ where E_0 denotes the ground-state energy. Second, we introduce a binning for ε and define $D(\varepsilon)$ as the number of inherent structures whose (excitation) energy density is in $[\varepsilon, \varepsilon + \delta\varepsilon]$, divided by $\delta\varepsilon$.
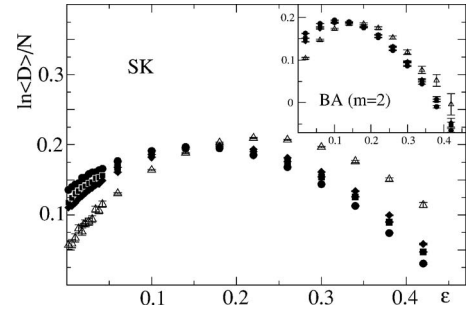

FIG. 6. The histogram of $N^{-1} \ln\langle D(\varepsilon)\rangle$ versus the excitation energy per spin ε for the SK model at $N=20$ (circles), 25 (squares), and 30 (diamonds). The triangles are the result of an $N \to \infty$ extrapolation. The bin size is 0.004 for $\varepsilon < 0.04$ and 0.04 otherwise. Inset: the same for the BA geometry, $m=2$.

Actually, it is convenient to renormalize $D(\varepsilon)$ by dividing it further by $\sqrt{N}$, as we now explain. Let $s(\varepsilon)$ denote the density of the "configurational entropy" so that

$$\langle N_s \rangle = \int d\varepsilon \langle D(\varepsilon)\rangle = \int d\varepsilon \exp[Ns(\varepsilon)]. \tag{9}$$

Assume that $s(\varepsilon)$ takes its maximum value at $\varepsilon = \varepsilon_m$. Hence at large N

$$\langle N_s \rangle \propto \int d\varepsilon \exp\left(N\left[s_0 + \frac{1}{2}s_2(\varepsilon - \varepsilon_m)^2\right]\right) \propto \exp(Ns_0)/\sqrt{N}. \tag{10}$$

However, our data, especially for the SK model, indicate that N_s increases exponentially with N, without any power prefactor. If so, there must be a factor $\sqrt{N}$ missing in Eq. (9), in the relation between $D(\varepsilon)$ and $\exp[Ns(\varepsilon)]$. Hence, we *redefine* $s(\varepsilon)$ by $s(\varepsilon) = N^{-1} \ln[\langle D(\varepsilon)\rangle/\sqrt{N}]$, which amounts to adding a finite size correction. To simplify the writing we hereafter absorb the factor $1/\sqrt{N}$ in the definition of $D(\varepsilon)$.

In Fig. 6 we show $s(\varepsilon) = N^{-1} \ln\langle D(\varepsilon)\rangle$ versus ε for the SK model [and in the inset for the BA ($m=2$) model] for $N =20, 25, 30$ as well as our $N=\infty$ extrapolation. The result of this extrapolation is close to that shown in Fig. 2 of Ref. [5], where it has been calculated in the mean field approximation, with two differences: it does not fall to zero when $\varepsilon \to 0$, and at the maximum it overshoots by 4.5% the exact value 0.1992…. However, our data have been collected at small N, and there are uncertainties with our extrapolation, so the agreement is actually pretty good. For the SK model, the extrapolated data are very well fitted by the parabola

$$s(\varepsilon) = 0.064\,167 + 1.2582\varepsilon - 2.7173\varepsilon^2. \tag{11}$$

This has a maximum at $\varepsilon \approx 0.23$ and vanishes at $\varepsilon \approx 0.51$.

An interesting quantity [independent of the normalization of $D(\varepsilon)$] is the ratio

$$R(\varepsilon) = \frac{\sqrt{\mathrm{var}[D(\varepsilon)]}}{\langle D(\varepsilon)\rangle}. \tag{12}$$

It is plotted in Fig. 7. In part (a) of that figure, we illustrate the behavior of $R(\varepsilon)$ for the BA geometry; the ratio is either
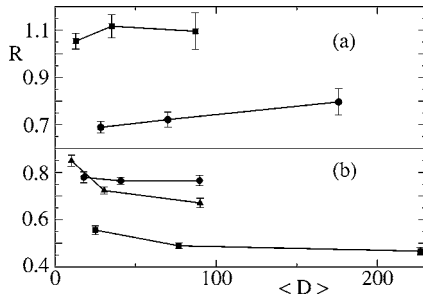
FIG. 7. The ratio $R = \sqrt{\langle D^2 \rangle - \langle D \rangle^2}/\langle D \rangle$ versus $\langle D \rangle$. (a) BA geometry: circles, $0 < \varepsilon < 0.16$; squares, $0.16 < \varepsilon < 0.32$; (b) SK geometry: circles, $0 < \varepsilon < 0.12$; squares, $0.12 < \varepsilon < 0.24$; triangles, $0.24 < \varepsilon < 0.36$.

FIG. 8. The barrier height B as a function of N. Circles, BA ($m=2$); stars, ER ($\langle k \rangle = 4$); squares, KR ($k=4$); up triangles, SK. The ordinate for the SK points has been shifted by -0.05 to make the figure less cluttered.

constant or increases slowly with $\langle D(\varepsilon) \rangle$ (and thus with N). A similar behavior is observed for other finite connectivity models. In part (b), we show $R(\varepsilon)$ for the SK model; the ratio is constant for the energy bin $[0, 0.12]$ and *decreasing* for larger excitation energies.

We also find that for all ε the shape of the distribution of $D(\varepsilon)$ is consistent with a log-normal law. If it were exactly log-normal, one would have

$$R(\varepsilon) = \sqrt{\exp[\sigma^2(\varepsilon)] - 1} \qquad (13)$$

where $\sigma^2(\varepsilon) = \mathrm{var}[\ln D(\varepsilon)]$.

If R keeps decreasing as $\langle D \rangle \to \infty$, the distribution of the density of inherent structures becomes more and more peaked, leading to

$$\lim_{N \to \infty} \ln\langle D(\varepsilon) \rangle / \langle \ln D(\varepsilon) \rangle = 1. \qquad (14)$$

This is what Bray and Moore find in the SK model for scaled excitation energies greather than 0.12, where as they claim the "metastable states are uncorrelated" [5]. In our data the fall of R is not as rapid as expected for a Poisson distribution, but the qualitative trend is similar. Unfortunately, we are unable to determine the critical energy very precisely; we can only state that our SK data are compatible with the results of Ref. [5].

IV. BARRIERS AND VALLEYS

A. Framework

The motivation for studying the scaling behavior of energy barriers separating inherent structures is well known: barriers that grow with N suggest a frozen (spin glass phase) at $T=0$ while finite barriers suggest a paramagnetic system. Here we focus on the energy barrier between the two ground states related by spin flip symmetry, which is expected to be the system's largest barrier. To go from one ground state to the other, all spins must be flipped and so we are interested in finding (a) the height of this barrier; (b) the appropriately defined distance between the ground state and this barrier state; and (c) the number of configurations that can be reached starting from one ground state while staying below this barrier height.
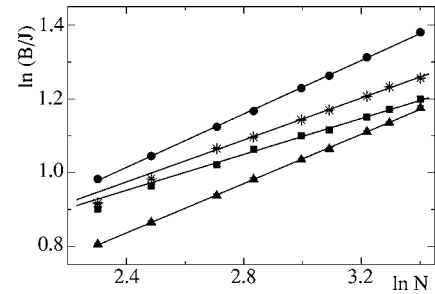
B. The barrier exponent

The energy landscape of a disordered and frustrated system generically has many valleys and energy barriers. Studies of barriers in spin glasses have focused almost exclusively on the SK case. (1) On the analytical side, Rodgers and Moore [6] performed an analysis of free-energy barriers near T_c and found an $N^{1/3}$ scaling. (2) Numerical investigations have estimated barriers *indirectly* via the relaxation times of Monte Carlo dynamics; the most recent simulations [7] give further support to an $N^{1/3}$ scaling. Very recently [21], a detailed study of barriers has been performed analytically for spin glasses on random graphs, but for a Hamiltonian involving three-spin interactions rather than the two-spin interactions of Eq. (1). In this work we shall study directly the energy barrier scalings for our four kinds of models, finding that the exponent depends on the nature of the underlying graph.

The energy barrier of interest is the one encountered when going from one ground state to its flipped counterpart. (Recall that our system has a global spin flip symmetry.) This energy barrier is expected to be the largest of all barriers. We determine it with our lid algorithm by letting the "water" proceed from the source (one of the ground states) up to the level given by the lid. When this level crosses the value B_J (the barrier for the instance under consideration), the water will flow all the way to the other ground state. B_J is a random variable (depends on the instance), so we have determined its moments and distribution as a function of N.

For each N and kind of model (KR, ER, etc.,), we have a numerical estimate of the distribution of B_J; define B as the energy for which this distribution is maximum. We show in Fig. 8 the log-log plots of B versus N for several of our models. (A similar plot can be obtained from the mean of B_J, but our definition of B leads to more stable results.) The numerical values of the slopes are collected in Table II.

The errors given in Table II are statistical only. The systematic errors are likely to be more important. We do not have them fully under control, but they can be roughly estimated as follows: the value of the exponent depends on the observable used to extract it, namely, the average of the barrier height or its modal value. Comparing these different observables, we expect the systematic error on the barrier exponents to be around ± 0.02. Similarly, the systematic error attached to the valley exponents discussed in the next section is tentatively estimated to be around ± 0.05.

TABLE II. The barrier and the valley exponents. Top numbers: slope of the least-square linear fit of $\ln B$ versus $\ln N$. Bottom numbers: slope of $\ln \ln N_{\text{wet}}$ versus $\ln N$. Only statistical errors are estimated.

	ER $\langle k \rangle = 4$	KR $(k=4)$	BA $(m=2)$	SK
Barrier exponent	0.285(4)	0.244(6)	0.363(4)	0.335(3)
Valley exponent	0.781(5)	0.708(5)	0.811(4)	0.644(6)

The result for the SK model gives strong support for the conjecture of a barrier scaling as $N^{1/3}$; note how well the data follow this scaling, starting even at such low values as $N = 10$. Power scaling is also very clear in the other models, though the scalings seem to set in a bit less early. For instance, our fits for KR graphs with $k=4$ lead to effective slopes that decrease as the lower range in N used for the fitting is increased; our best estimate for the exponent is then 0.244(6), a result completely incompatible with $1/3$. We thus conclude that barrier exponents depend on the nature of the underlying graphs. It is manifest that for the homogeneous finite connectivity models studied here the barrier exponent is significantly lower than for SK (a similar result is found, e.g., for ER graphs with average degree equal to 3). The inhomogeneous BA models behave differently, more like the SK model, and there is no indication in our data that such a trend is due to finite size effects, although this possibility cannot, of course, be totally excluded.

In contrast to the quantity N_s, we find that B_J is self-averaging, i.e., its relative fluctuations *decrease* and go to zero as N grows:

$$\frac{\sqrt{\text{var}[B_J]}}{\langle B_J \rangle} \propto N^{-\gamma} \quad (15)$$

with the exponent γ ranging from about 0.14 (SK model) to 0.30 (KR $k=4$ model). From such a self-averaging behavior, one may guess that B_J is to some extent a sum of many small barrier heights.

C. The valley exponent

Let us consider now the number of configurations that are wetted just before the barrier is reached. Since the procedure wets all reachable configurations in its search of the pass, this number measures the size of the valley or, stated differently, the size of the basin of attraction of the ground state. It turns out to depend strongly on the geometry of the model. Thus, for example, at $N=30$, the average number of wet sites is 2940 in the SK and 40 000 in the BA ($m=2$) model.

Each wet site represents a configuration of the system. We observe that *nearly all* configurations or their associated flipped partners whose excitation energies are lower than B_J, the height of the barrier, get wet. This is true for all models and says that B_J is probably as expected the largest energy barrier in the system.

We define N_{wet} as the most probable number of wet configurations when the lid finally reaches the barrier. (It is thus extracted from all of our instances at a given N, just as B was.) We find the simple scaling property

$$N_{\text{wet}} \propto \exp(cN^\nu) \quad (16)$$

where c is a numerical constant. The value of the "valley exponent" ν is always below 1 (see Table II). (Note that we have also performed the analysis using the mean number of wet configurations rather than the modal value and the results are very similar.)

Let us present a heuristic argument for why a stretched exponential as in Eq. (16) is natural. The wet sites represent configurations with energies differing relatively little from the ground-state energy E_0, the extreme energy of the system, proportional to N. A simple guess is that the (microcanonical) entropy density $s(e)$ vanishes as

$$s(e) \sim A(e - e_0)^\alpha \quad (17)$$

as $e = E/N$ tends toward the ground-state energy density $e_0 = E_0/N$. (Here A is a constant and α is a positive exponent.) Then the probability that a configuration has energy density e is

$$P(e) \propto \exp[NA(e - e_0)^\alpha] \quad (18)$$

for e tending toward e_0. Using the fact that for configurations below the energy barrier B_J, $e - e_0$ becomes infinitesimal as $N \to \infty$, the number of wet configurations is

$$N_{\text{wet}} \propto \int_{e_0}^{e_0 + B/N} P(e)de \propto \int_0^{N^\beta} \exp[AN(z/N)^\alpha]dz \quad (19)$$

where β is the barrier exponent. For large N the integral is dominated by the upper limit and one gets (16) with $\nu = \alpha\beta - \alpha + 1$. Using our measurements of β and ν, this gives values of α ranging from about 0.3 to approximately 0.5. Related considerations can be found in Ref. [22].

D. Ground state to barrier state distances

The idea of our algorithm was briefly explained in Sec. II C. Along the shortest path from the ground state to the saddle point (pass), a given spin can get flipped more than once. This path has to avoid multiple obstacles and can be quite tortuous. It is not explicitly constructed by our simple "wetting" algorithm, which merely identifies the location of the saddle point in the configuration space. Once this is done, one easily finds the Hamming distance separating the ground state and the saddle point, i.e., the barrier state. The mirror state is then also easily identified.

The distribution of the Hamming distances separating the ground state from the pass is shown in Fig. 9; the distribution is the least broad for the SK model and the broadest for regular graphs with $k=3$. Other models, including the BA one, exhibit intermediate behaviors.

Detailed investigations show that just before the lid energy is reached, in almost all cases the two passes (related by a global spin flip) are *both* on the boundary of the wet sites. From this fact, we can reach a useful qualitative picture of the energy landscape. Recall that each ground-state valley corresponds to a connected cluster of vertices of the N-dimensional Boolean hypercube. Generically, two barrier configurations, related by a global spin flip symmetry, form the "passes" where the two valleys "touch." This is very
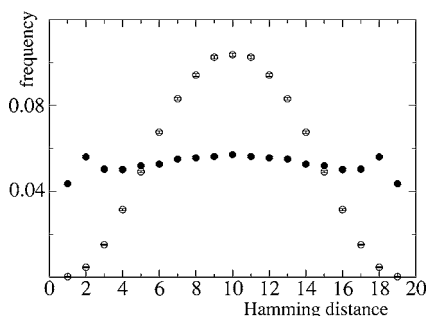
FIG. 9. The normalized Hamming distance distribution separating the Boolean hypercube sites representing the ground state and one or the other saddle point (for $N=20$); empty circles, SK; full circles, KR ($k=3$).

different from what happens in a one-dimensional energy landscape. There, if one has two passes, then the two valleys do not touch; instead an intermediate zone separates them. In our systems, only on very rare occasions (at the level of about 1 in 1000) have we found that a valley is in contact with just one pass. Thus in the generic case, the valley to valley barrier is associated with two passes, both in contact with each ground-state valley.

V. SUMMARY AND CONCLUSION

Many complex systems can be represented by a complicated network connecting a large number of simpler subunits. The knowledge of the network architecture is an important piece of information, but it does not tell much about the system's global behavior. Instead, it is frequently the energy landscape that is relevant for the cooperative behavior of systems consisting of many interacting units (see Refs. [23,24]). An interesting question is, what is the relation between the system's behavior and its design? between the shape of its energy landscape and the topology of its network? This question motivated our investigation.

Our study focuses on spin glasses that are archetypes of complex systems. A major conclusion of our work is that reliable results can be obtained from quite small systems, provided the enumeration of configurations is exhaustive: for example, in the SK model we reproduce correctly the first three significant digits of the quantity $N^{-1}\ln\langle N_s\rangle$ (which has been calculated analytically long ago). The techniques we use are relatively straightforward, but allow us to unveil essential aspects of the energy landscape in these systems as we now summarize.

We find that the distribution of the number of inherent structures is log normal in all examined models. This usually reflects the extensivity of local excitations and their low level of correlations, a property that should hold in a variety of other models with finite connectivity.

We further observe a simple scaling behavior with the number of spins of the size of the ground-state basin of attraction and of the height of the energy barrier between the two degenerate ground states, respectively. However, the cor-

responding exponents are not universal. For instance, the barrier exponent in the SK model (equal to $1/3$) is definitely larger than the exponents found in all models where underlying graphs are homogeneous. Similar results hold for the valley exponent. Nevertheless there is some level of universality: the exponents seem to be independent of the underlying J_{ij} distribution. For instance in the SK model, the barrier exponent is, within the limits of our systematic error, the same when the J_{ij} are generated from an exponential distribution and from the Gaussian distribution; we have also checked this for the KR $k=4$ model, though finite size effects there were stronger. We find this level of universality to arise also for the valley exponent.

On the whole, the qualitative behavior of the models we considered is very similar, with one notable exception: the variance of $\ln N_s$ *decreases* with increasing N in the SK model, while it *increases* in all models with finite connectivity graphs. This difference is quite essential and signals a qualitatively different nature of this complex system, arguably due to the absence of small scale excitations.

In spite of their qualitatively similar behavior, the models are very different quantitatively. The seemingly small differences between parameters plotted in Figs. 2 and 3 translate into large differences of multiplicity distributions. For instance, the size of the basin of attraction in the BA ($m=2$) model is one order of magnitude larger than in the model where graphs are regular with degree 4, etc.

This paper is an exploratory one and many questions remain open. We showed in Sec. IV D that the two ground-state valleys had a connectivity property that was nonexistent in one-dimensional energy landscapes; it would be of interest to understand the nature of passes between more general valleys in these systems. It would also be worthwhile to explore the topology of the graph associated with the inherent structures. Such *inherent networks* have been constructed, for example, for certain atomic clusters [25,26]. We would like to see whether there is some relation between the underlying topology of the model and the topology of its inherent network. However, the nontrivial definition of the latter for a discrete system like a spin glass requires a separate discussion; this issue is beyond the scope of the present paper.

[1] C. De Dominicis and Y. Goldschmidt, J. Phys. A **22**, L775 (1989).

[2] L. Viana and A. J. Bray, J. Phys. C **18**, 3037 (1985).

[3] D. H. Kim, G. J. Rodgers, B. Kahng, and D. Kim, Phys. Rev. E **71**, 056115 (2005).

[4] D. Sherrington and S. Kirkpatrick, Phys. Rev. Lett. **35**, 1792 (1975).

[5] A. J. Bray and M. A. Moore, J. Phys. C **13**, L469 (1980).

[6] G. Rodgers and M. Moore, J. Phys. A **22**, 1085 (1989).

[7] A. Billoire and E. Marinari, J. Phys. A **34**, L727 (2001).

[8] J. Dall and P. Sibani, Eur. Phys. J. B **36**, 233 (2003).

[9] T. Klotz and S. Kobe, J. Phys. A **27**, L95 (1994).

[10] P. Sibani and P. Schriver, Phys. Rev. B **49**, 6667 (1994).

[11] P. Sibani, R. van der Pas, and J. Schoen, Comput. Phys. Commun. **116**, 17 (1999).

[12] L. Barabasi and R. Albert, Science **286**, 509 (1999).

[13] P. Sibani, J. C. Schön, P. Salamon, and J. O. Andersson, Europhys. Lett. **22**, 479 (1993).

[14] T. Li, Phys. Rev. B **24**, 6579 (1981).

[15] B. Derrida and E. Gardner, J. Phys. (France) **47**, 959 (1986).

[16] C. Dasgupta, S. K. Ma, and C. K. Hu, Phys. Rev. B **20**, 3837 (1979).

[17] F. Tanaka and S. Edwards, J. Phys. F: Met. Phys. **10**, 2769 (1980).

[18] C. De Dominicis, M. Gabay, T. Garel, and H. Orland, J. Phys. (France) **41**, 923 (1980).

[19] D. S. Dean, Eur. Phys. J. B **15**, 493 (2000).

[20] P. W. Anderson, in *Ill-Condensed Matter*, edited by R. Balian *et al.*, Proceedings of the Les Houches Summer School of Theoretical Physics, XXXI, 1978 (North-Holland, Amsterdam, 1979).

[21] A. Montanari and G. Semerjian, Phys. Rev. Lett. **94**, 247201 (2005).

[22] T. Klotz, S. Schubert, and K. H. Hoffmann, Eur. Phys. J. B **2**, 313 (1998).

[23] F. H. Stillinger and T. A. Weber, Science **225**, 983 (1984).

[24] *Proceedings of the 16th Annual International Conference of the Center for Nonlinear Studies, Los Alamos*, edited by H. Fraunfelder *et al.* [Physica D107, 117 (1997)].

[25] J. P. K. Doye, Phys. Rev. Lett. **88**, 238701 (2001).

[26] J. P. K. Doye and C. P. Massen, Phys. Rev. E **71**, 016128 (2005).